



Nuclear Materials Authority
P.O.Box 530 Maadi, Cairo, Egypt

DOAJ DIRECTORY OF
OPEN ACCESS
JOURNALS

ISSN 2314-5609

Nuclear Sciences Scientific Journal

11, 1-23

2022

<https://nssi.journals.ekb.eg>

RADIOLOGICAL AND ENVIRONMENTAL IMPACTS OF EL SELA-QASH AMER GRANITES, SOUTH EASTERN DESERT, EGYPT

SAMEH Z. TAWFIK; MOHAMED A. SHAHEEN and MOSTAFA S. ELSETOUHI

NUCLEAR MATERIALS AUTHORITY, P.O. BOX: 530, MAADI, CAIRO

ABSTRACT

El Sela area is mainly covered by ophiolitic mélangé (Sul Hamed), biotite granite, two-mica granite (El Sela), muscovite granites (Qash Amer), and cross cut by microgranite dolerite and bostonite dikes as well as quartz and jasper veins. These granitic rocks are hydrothermally altered, especially around El Sela ENE-WSW shear zone, that causing hydrothermal alterations accompanied by radioactive mineralization. These rocks are mainly composed of alkali feldspar, quartz, muscovite, and biotite with zircon, fluorite, apatite and iron oxides as an accessory minerals. The radioactive minerals are represented by uranophane, autunite, meta-autunite and phurcalite which are restricted in the highly sheared microgranite, dolerite dikes as well as jasper veins. Uranium contents (eU) range from 10.1 to 17.7 ppm at Qash Amer with their thorium contents (eTh) vary from 5.8 to 22.7 ppm. El Sela granites have uranium contents (eU) range from 6.4 to 19.7 ppm with equivalent thorium content (eTh) range between 14.0 and 44.9 ppm. The eU-eTh, (eU/eTh)-eU and eU-[eU+(eTh X 3.5)] diagrams show depletion of uranium for both the Qash Amer and El Sela granitic samples, suggesting that uranium may be leached out of the original rock towards the ENE-WSW and NNW-SSE shear zones. The migrated uranium (Um) amount was calculated and indicated as either migration out or migration in at Qash Amer and El Sela granites, mostly to the shear zone cutting through the area. Absorbed Dose Rate (D), annual effective dose equivalent (AEDE), radium equivalent activity (Raeq), external (Hex) and internal (Hin) hazard index, in addition to activity gamma index (I_γ) caused by gamma emitter natural radionuclide were determined from the obtained values of ²³⁸U, ²³²Th and ⁴⁰K. Most of the studied samples have radiological parameters values higher than the international recommended values suggesting that El Sela and Qash Amer granitic rocks are hazardous and not recommended for use as ornamental stones with respect to workers and human beings.

INTRODUCTION

The Pan-African orogenic event in Egypt ended at about 615 Ma, and subsequent crustal uplifting and extensional collapse occurred within the 610–550 Ma time span (Stern, 1994; Greiling et al., 1993). The basement complex in the Eastern Desert of Egypt is divided into three lithologically and structurally distinct domains: North Eastern

Desert (NED), Central Eastern Desert (CED) and South Eastern Desert (SED), (Stern and Hedge, 1985). Lithologically, there are higher number of granitic occurrences in the NED and SED than in the CED; ophiolites are absent in the NED; and the greatest occurrences of rocks with strong oceanic affinities are exposed in the CED. Granitic rocks constitute about 60% of the basement

outcrops in the Eastern Desert of Egypt. The Egyptian granitic rocks divided into an older (850–614 Ma), also referred to as grey or syn-to late-orogenic, calc-alkaline diorite to granodiorite assemblage, and a younger (610–550 Ma), post-orogenic, alkali granite, syenogranite, and monzogranite association (Hassan and Hashad, 1990; Stern and Gottfried, 1986; Beyth et al., 1994). Older granites constitute about 27%, whereas the younger granites about 30% of the Egyptian granites. Relative abundance of younger granites to older granites increases from 1:4 in the south to 1:1 in the north of Eastern Desert and 12:1 in Sinai (Bentor, 1985). Granitic rocks are considered the main rocks hosting U-mineralization in many parts of the world. Uranium existing in granites can be divided into two categories; primary uranium and secondary uranium (Jiashu and Zehong, 1982). The first is formed during magma crystallization, while the latter is precipitated in various geological events later from dissolved and transported uranium, which comes from the primary uranium. The secondary uranium can be subdivided into three types: a) absorbed uranium in altered minerals such as montmorillonite, chlorite and limonite; b) interstitial uranium at the grain boundaries, formed as a result of hydrothermal solution migration along the interstices of minerals in granites; and c) uranium in microfractures, the formation of this kind of uranium takes place during the circulation of hydrothermal solutions after the deformation of rocks. Most of Egyptian uranium occurrences in the younger granites as Gabal Um Ara (Ibrahim, 1986; Abdalla et al., 1994), Gabal Gattar (Roz, 1994), while the vein type is dominant in other areas such as; Gabal El Missikat, Gabal El Erediya (Abu Dief, 1985 & 1992 and Hussein et al., 1986; Abdel Naby, 2008; El Mezayen et al., 2017), and Gabal El Sela (Assaf et al., 1996; Ibrahim et al., 2005). These areas were studied geochemically (e.g. El-Nisr et al., 2002; Khalaf, 2005, Abdel Gawad 2018), mineralogically (e.g. Rashed, 2001; Gaafar,

2005; Mira and Ibrahim 2009; Shahin, 2011 and 2014; Abdel Gawad et al., 2015, Abdel Gawad and Ibrahim 2016) and structurally (Ali, 2013).

El Sela area lies in south Eastern Desert of Egypt covering an area about 70 km² of the basement rocks. Recent studies show that most granites in the area are composed of multiple phase injections of highly variable sizes, not always co-genetic and each of them may have highly variable metallogenic potential (Ibrahim, 2002). Such a conception has a very important consequence because the mineralization may be genetically only related to specific magma intrusion phase within a large granite complex as shown in Kab Ameri granite, Central Eastern Desert of Egypt (Abdel Meguid et al., 2003; Ibrahim, et al 2005; Gaafar et al., 2006) and Saint Sylvester granite in the French Massif Central for vein type uranium mineralization (Cuney et al., 1989).

This work aims to measure the radioactivity of El Sela granitic rocks which could be used as building materials to evaluate the probable radiological hazards that imposed on the human beings.

MATERIALS AND METHODS

The granitic samples collected from the study area were prepared as thin sections and studied by the transmitted polarized microscope (Olympus BX53).

Mineral separation and identification were carried out at the Laboratories of the Nuclear Materials Authority (NMA). The heavy liquids separation technique using bromoform of specific gravity 2.85 gm/cm³ was used to concentrate the heavy minerals followed by magnetite separation using the hand magnet, then the left heavy portion was subjected to magnetic fractionation by the Frantz isodynamic magnetic where several fractions are obtained at variable amperes (0.2, 0.5, 0.7, 1, and 1.5 amperes). Each of these fractions contained its own character-

istic minerals that were identified by the Environmental Scanning Electron Microscope (ESEM).

A total number of 80 sites (40 for El Sela granites in El Sela area and 40 for Qash Amer granites, Southeastern Desert, Egypt) were considered to investigate their natural radioactivity due to ^{238}U (ppm), ^{232}Th (ppm) and ^{40}K (%). The radiometric measurement was carried out in the field using in-situ γ -ray spectrometer, GS-256 (designed by Geofyzika Brno-Czech Republic) with a 3×3 sodium iodide (Thalium) [NaI (TI)] crystal detector and in addition to a system work with the GPS units.

The measurements are based on the detection of γ -radiation emitted in the decay of ^{214}Bi (^{238}U series) at 1.76 Mev, ^{208}Tl (^{232}Th series) at 2.41 Mev, while primary decay of potassium ^{40}K (1.46 MeV) is measured directly. The determinations of uranium and thorium are based on the assumption that the daughter nuclides are in equilibrium with the parent nuclides that is none of the intermediate

steps in the decay series has been disrupted. Consequently, the deduced amounts of uranium and thorium are equivalent to what would be in equilibrium with the measured radioactivity of the bismuth or thallium isotopes (Killeen and Cameron, 1977). Therefore the term 'equivalent' or its abbreviation 'e' is used to indicate that equilibrium is assumed between the radioactive daughter isotopes monitored by the spectrometer, and their respective parent isotope. Based on replicate analyses, the precision of the determinations was $\pm 10\%$.

GEOLOGIC SETTING

El Sela granites and Qash Amer (QA) are located 25 km west of Abu Ramad city close to the Sudanese border (Fig. 1). El Sela and Qash Amer areas are characterized by rugged topography with low to high relief and comprises different rock types of the basement complex. They are chronologically arranged by serpentinite and related rocks, metagabbros, pillowed metabasalt, metavolcanics, biotite granite, two-mica granite, muscovite granite,

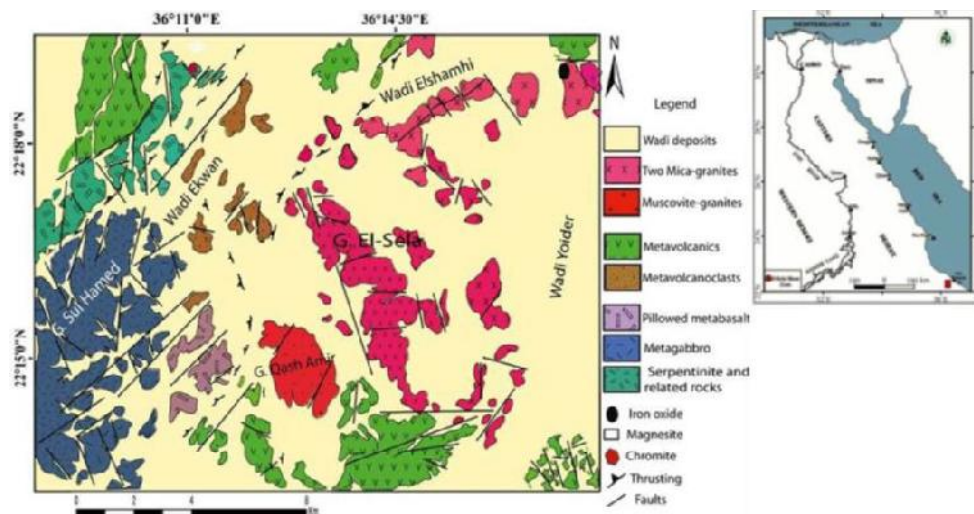


Fig. 1 : Location and Geologic map of G. El Sela (Modified after Abu El Laban, 2002; Lasheen, 2019)

microgranite, dolerite, bostonite dikes and quartz and jasper veins in decending manner. Post-granitic dikes are mostly injected along ENE-WSW and/or NNW-SSE to N-S directions which represent the most important tectonic trends in the study area (Fig. 2).

The basement complex of El Sela area is represented by Sul Hahmid serpentinite talc carbonate structurally inter slices with layered

pyroxene gabbro, ophiolitic basalt and calc alkaline metavolcanics and related volcani-clastic sediments. The calc alkaline metavolcanics are intruded by El Sela and Qash Amer granitic rocks.

Biotite granite of El Sela area is represented by huge granitic exposure trends NNW-SSE displaying an elongated belt (9 x 3 km). It is red to reddish pink color, massive, and

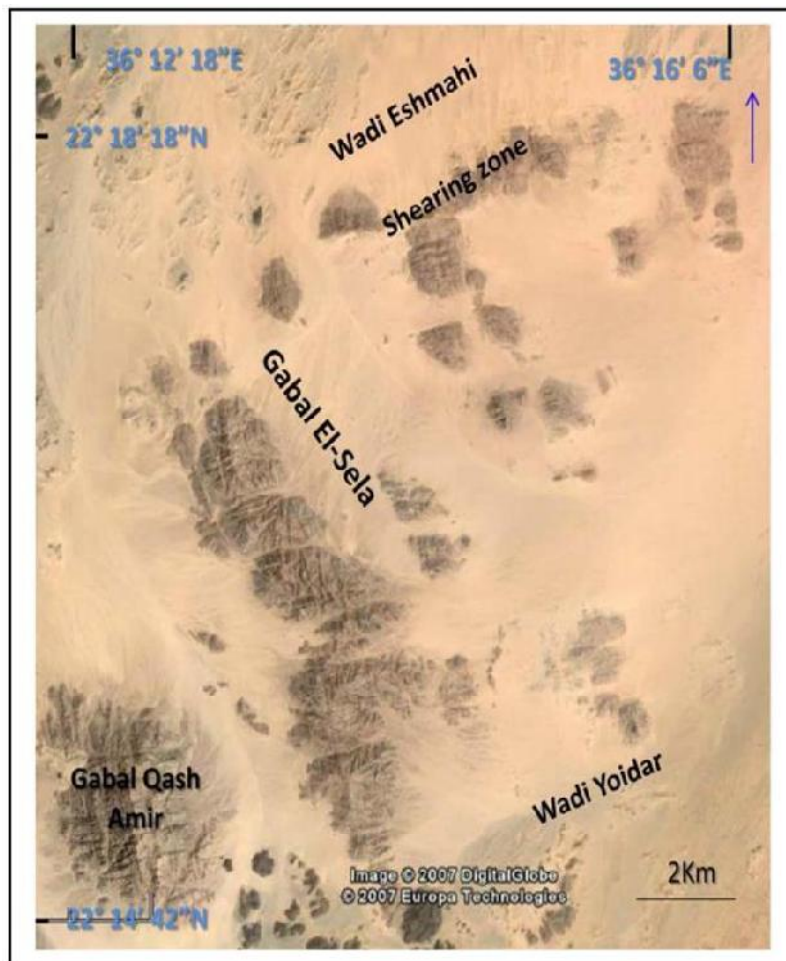


Fig. 2 : Land Sat image for G. El Sela- G. Qash Amer. South Eastern Desert, Egypt (After Abu Zeid, 2020)

exhibits low to moderate relief, medium- to coarse-grained. This granite implies cavernous, highly weathered, exfoliated, fractured and jointed surfaces. It is composed mainly of quartz, k-feldspar, plagioclase, and biotite. Fe and Mn-oxides represented by magnetite, hematite, goethite, and pyrolusite minerals filling fissures and joints. The rock contains xenocrysts of black colors of metavolcanics. The biotite granite was intruded by the two-mica granite with strong and sharp intrusive contact.

The two-mica granites occupy the major part of the studied area displaying the remnants of circular and/or arc-shaped granitic plutons trending ENE–WSW and NNW–SSE. These granites are usually medium- to coarse-grained and characterized by the hypidiomorphic granitic textures. Granite plutons are divided into several bodies separated by sandy corridors with highest peaks rise to as high as 557 m (above sea level). Two-mica granites are pink to pinkish grey colors, composed essentially of quartz, K-feldspar, plagioclase, biotite and muscovite.

The Qash Amer granite locates to the east of Gabal El Sela, represents a small (3 x 2 km) oval body surrounded by wadi sediments. Gabal Qash Amer has a higher relief than Gabal El Sela. Granites of Qash Amer are strongly weathered, exfoliated, jointed, pale pink, leucocratic, medium to coarse-grained, whitish to pink in color and composed mainly of muscovite granites. These rocks are composed essentially of quartz, K-feldspar, plagioclase, biotite and muscovite. Garnet, manganese and iron oxides are the main accessories as disseminations and fracture fillings indicating its high degree of differentiation. They intrude serpentinite rocks and metavolcanics as well as biotite granite.

El Sela granites are dissected by two perpendicular shear zones. First shear zone extends ENE–WSW with about 1.5 km in length and ranges between 5 to 40 m in width extending 6 km in the eastern part with nar-

row width varies between 3 to 5 m. From the structural point of view, shear zone is dissected by the NW–SE dextral strike-slip faults, NNW–SSE, NNE–SSW and N–S sinistral strike-slip faults. The ENE–WSW shear zone is characterized by moderate relief, highly tectonized, altered and enriched in secondary visible U-mineralization and pyrite megacrysts. This shear zone is characterized by invading of microgranite, dolerite dikes, as well as quartz and jasper veins.

Microgranite dike is injected into the two-mica granite along the ENE–WSW shear zone and dipping 72° – 83° S (Fig. 3). This dike is very fine-grained, ranging in width between 3 and 20 m and extends 6 km SW from the northern margin of El Sela plutons. Microgranite is sheared, jointed and affected by acidic and/or alkaline fluids such as phyllic, argillic and hematization. Dolerite dikes have ENE–WSW and NNW–SSE trends. The first trend in which dolerite is parallel to the first shear zone, strikes $N75^{\circ}E$ and dipping 68° – 81° SW, adjacent and/or parallel to microgranite dike in the main shear zone of the mapped area. These dikes are highly altered and having cavities that filled with secondary U-mineralization and pyrite megacrysts (Fig. 4 & 5).



Fig. 3 : Photograph showing sheared altered microgranite trending ENE-WSW

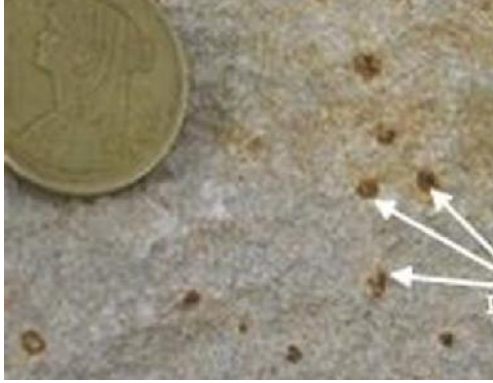


Fig. 4 : Photograph showing visible pyrite megacrysts



Fig. 6: Photograph showing argillic alteration enriched by secondary U-mineralization in altered dolerite dike along NNW-SSE shear zone



Fig. 5: Photograph showing visible uranophane refilling cavities of dissolved pyrite megacrysts

Bostonite dikes invade granitic plutons along the N-S and NNE-SSW tectonic trends (Fig. 7). They are usually fine-grained, reddish brown, sheeted, and range in thickness from 0.5 to 2 m. These dikes are mainly composed of microcline, albite, quartz, aegirine and iron oxides.

Milky and white quartz veins dissected the host two-mica granite along the main shear zone trending ENE-WSW (Fig. 8). These veins are barren, highly brecciated and vary

The Second shear zone extends NNW-SSE for a short distance (100 m). Dolerite dikes range in thickness 1 m to 1.5 m thick and act as good trap for visible U-mineralization. They invade the first shear zone in perpendicular trend. The second mineralized dolerite trend strikes N-112° and dips 58° W. The intensity of radioactivity and mineralization in the second shear zone are very strong and more pronounced than the first one. Visible uranophane and violet fluorite minerals are recorded in the second sheared dolerite dikes (Fig. 6).



Fig. 7: Photograph showing the NW-SE strike slip fault (right lateral) cross cut N-S bostonite dike



Fig. 8: Photograph showing the ENE-WSW jasper vein invades the contacts between two-mica granite and microgranite

between 1 to 4 m in width. The milky quartz veins were dissected by grey and reddish black jasper veins. Jasper veins are mineralized and contain visible uranophane minerals and pyrite megacrysts. They were jointed, brecciated and varies in their thickness between 0.5 and 1 m.

Episyenitization, Hematitization, kaolinization, illitization are the main alteration processes in the area. The field observations and detailed mapping indicate that the tectonic history of the area forms a conspicuous feature as it was affected by several tectonic events. The main tectonic trends affect the studied granite are ENE-WSW and NNW-SSE fault sets with contemporaneous different injections. The emplacement of these injections along the fault zones were associated with high potential fluids which are indicated by the alteration halos. These events are started by the emplacement of the two-mica granite and muscovite granite, and continued by the ENE-WSW trend that was activated many times. These activations were contemporaneous with or followed by the emplacement of microgranite dikes in ENE-WSW trends. Dolerite dikes having ENE-WSW and NNW-SSE trends while bostonite dikes having N-S trend and the multi-color of quartz vein injections along

ENE-WSW trends. The field studies indicated that the granitic rocks suffered from hydrothermal alterations, especially around El Sela shear zone, which intruded by multi injections of microgranite, dolerite and bostonite dikes as well as quartz veins along ENE-WSW trend causing hydrothermal alterations affected the host two-mica granite, microgranite and dolerite dikes and was accompanied by visible secondary U-mineralization and megacrysts of pyrite crystals (Figs. 4-6).

PETROGRAPHY

Qash Amer syenogranite is medium- to coarse-grained characterized by hypidiomorphic texture. QA is a muscovite \pm garnet leucogranite. It consists mainly of potash feldspars, quartz, plagioclase and mica.

The granitic rocks in El Sela area can be distinguished into two types. The first is coarse grained intruded by the second fine- to medium-grained granite. Microscopically the coarse-grained granite is composed essentially of alkali feldspar, quartz, and biotite \pm muscovite. Zircon, monazite, fluorite, apatite and iron oxides are the main accessory minerals. Quartz presents as subhedral to anhedral crystals and shows andulose extinction reflecting the effecting tectonics. It occurs as large crystals and/or small crystals filling the interstitial spaces between the plagioclase and microcline. Orthoclase and microcline crystals represent the potash feldspar. Orthoclase shows simple twinning, while the microcline is characterized by corroded cross-hatching. Some crystals show sericitization along the periphery. Plagioclase is subhedral to euhedral crystals, cracked and partly sericitized. They are altered where alteration causing masking for lamellar twinning. Biotite occurs as flakes with pale to dark brown pleochroism. Muscovites present as small flakes and as alteration products of biotite.

The second fine- to medium-grained granites are composed essentially of

quartz, K-feldspar plagioclase, biotite and muscovite. Garnet, zircon and iron and manganese oxides are the main accessories.

Quartz occurs as medium to fine subhedral cracked crystals, with wavy extinction. These crystals have different grain sizes ~2.0 mm length and width. The potash feldspars are microcline, orthoclase and perthite. Microcline crystals are partly corroded crosshatched, sericitized and silicified (Fig. 9). Orthoclase crystals are euhedral to subhedral with carlsbad twinning. Perthite is few and shows subhedral crystals with vein and patch type perthitic intergrowth. Plagioclase is euhedral to subhedral cracked crystals, partly with corroded lamellar twinning, and sericitized. Sericitization presents in the crystals core (Fig. 10). It ranges from albite to oligoclase. Occasionally it shows clear zoning textures (Fig. 11).

Biotite occurs as flakes with pale to dark brown pleochroism. Some biotite crystals shows black haloes which may be due to radioactive minerals. Muscovite occurs as irregular flakes filling the interstitial spaces between these minerals. Garnet occurs as honey color, euhedral crystals and high relief. The presence of this mica may indicate of highly fractionated rare metal granites.

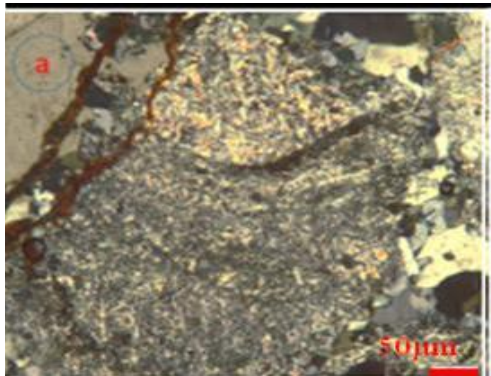


Fig. 9: Sericitized and silicified crystal of feldspar

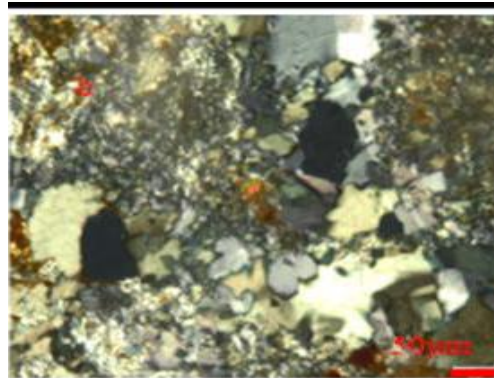


Fig. 10: Euhedral zircon associating secondary quartz (reworked silica)

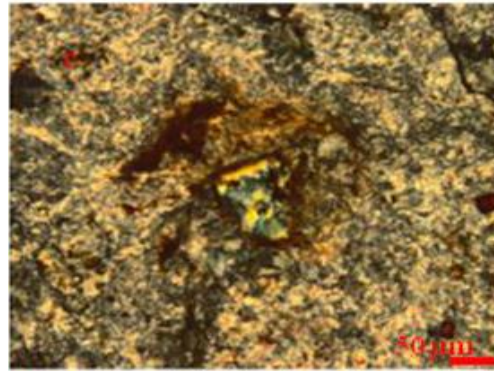


Fig. 11: Euhedral crystal of metaautunite in sericitized feldspars

Zircon, uranophane, autunite and metaautunite are the main accessories. Sometimes, autunite and metaautunite are replaced by iron oxides (Fig.12-14).

RADIOACTIVE MINERALS

Uranium Bearing Minerals

Accessory minerals are represented mainly by zircon, and fluorite. Zircon occurs as small subhedral to euhedral crystals. It is also observed as inclusions in quartz, biotite, feldspars and chlorite. Some zircon

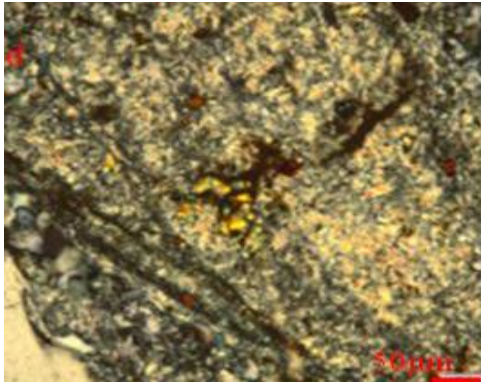


Fig.12 : Euhedral crystal of autunite associating altered feldspar

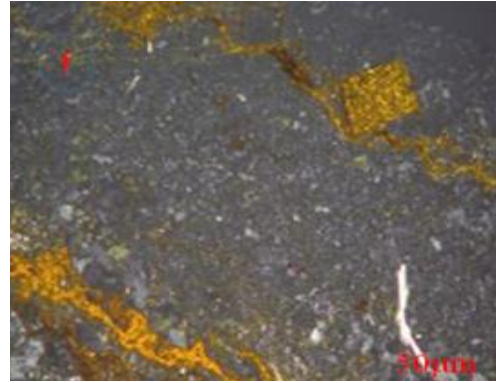


Fig. 14: Veinlets of iron oxides feeding and replacing euhedral crystal of metaautunite

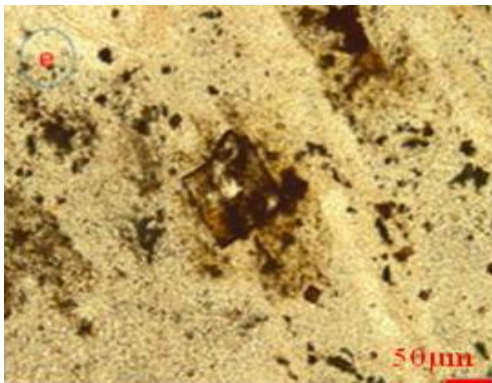


Fig. 13 : Partial replacement of metaautunite by iron oxides

crystals are occasionally metamict and surrounded by strong pleochroic haloes due to the radioactivity effects. Fluorite occurs as colorless and or as deep violet to black fluorite associating radioactive mineralization (Fig. 15a&b).

Secondary Uranium Mineral

Secondary uranium minerals are represented by uranophane (Fig.15c), autunite (Fig.16), meta-autunite $[Ca(UO_2)_2(PO_4)_2 \cdot 2-6H_2O]$ and phurcalite $(Ca_2(UO_2)_3O_2(PO_4)_2 \cdot 7(H_2O))$, (Fig. 17), which are the secondary uranium minerals in highly radioactive type of the

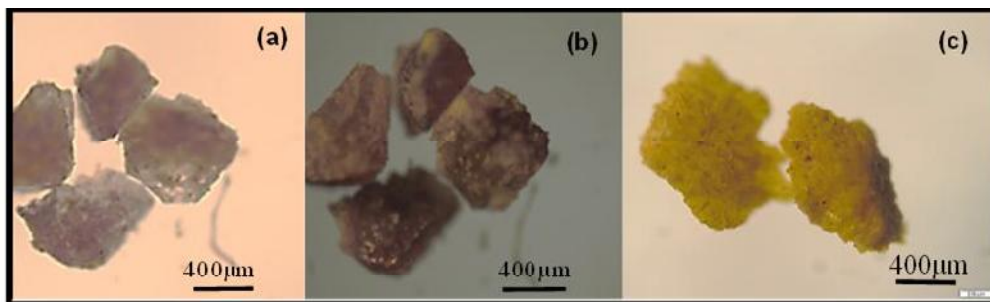


Fig. 15 : Fluorite (a & b), uranophane (c)

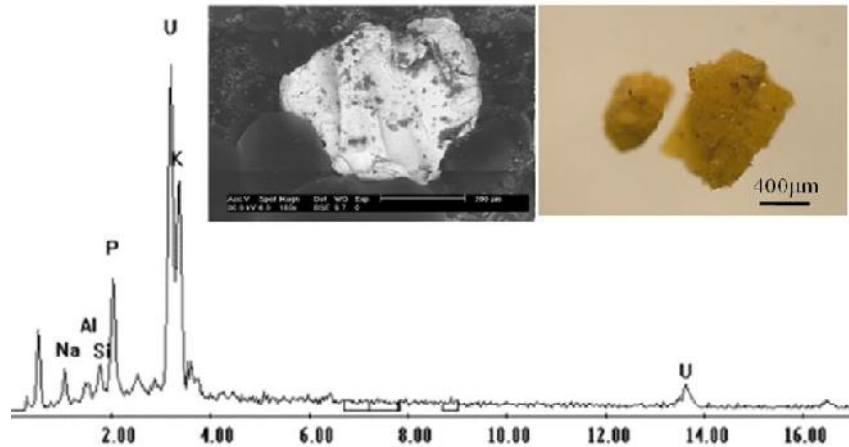


Fig. 16: EDX analysis, BSE and binocular image of autunite

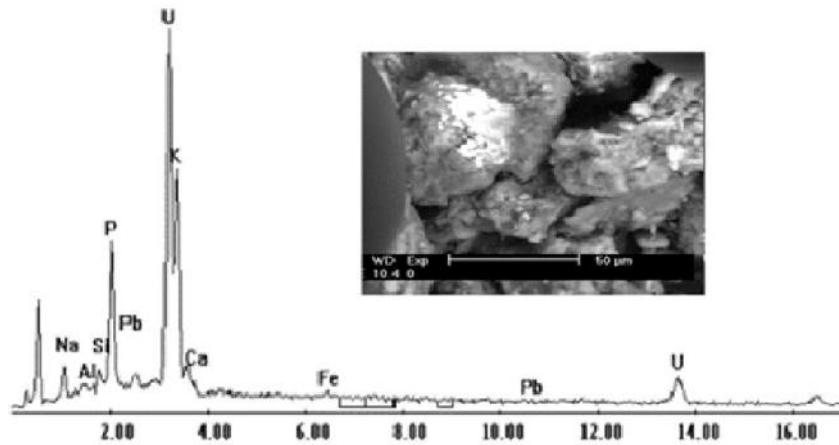


Fig. 17: EDX analysis and BSE image of phurcalite

studied granites (altered microgranite). The aggregates of autunite and meta-autunite are soft and consist of lemon yellow to greenish yellow small crystals with a micaceous habit. Occasionally meta-autunite is found as tabular square crystals often in parallel growths and terminated by bipyramidal forms.

Radioactivity Ratios

The wide ranges of eU/eTh ratio of Qash

Amer granites (0.66–2.14) and eTh/K ratio (5.03–9.36) indicate that they have a very high U potential mobilization and its ratios is not normal and form anomalous zones (Saleh et al., 2019).

The eU-eTh, (eU/eTh)-eU and eU-[eU+(eTh*3.5)] diagrams (Figs.18-21) show depletion of uranium for both the Qash Amer and El Sela granitic samples. Uranium was leached out of the original rock towards the

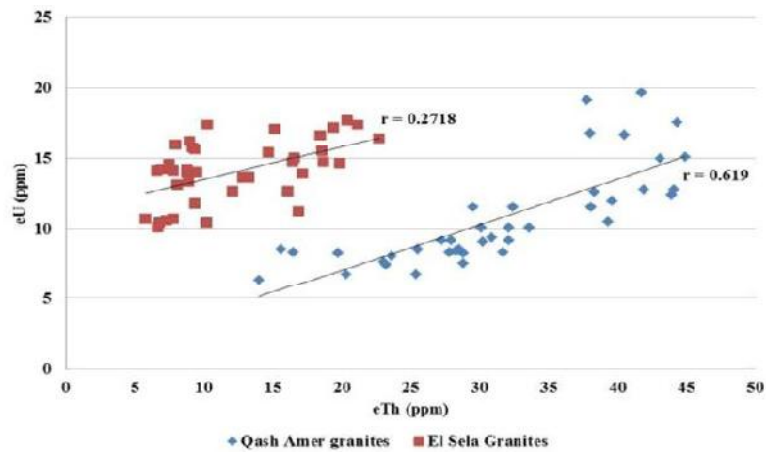


Fig. 18: eTh-eU binary diagrams for QA and El Sela granites

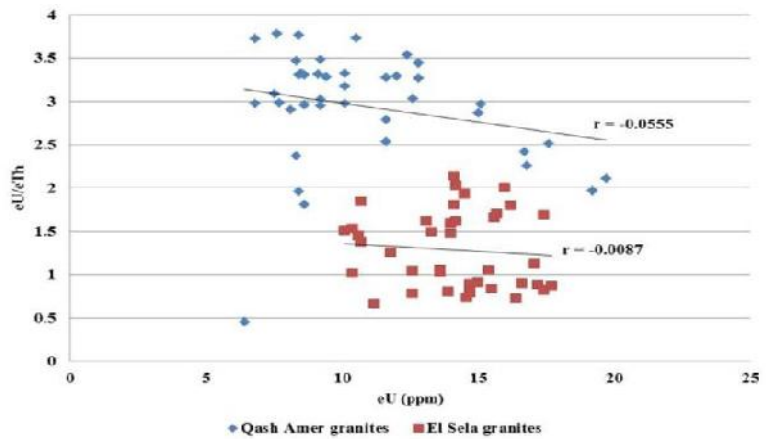


Fig. 19: eU-(eU/eTh) binary diagrams for QA and El Sela granites

shear zone.

Mobilization and Migration of Uranium

Uranium is the most expected element to be mobilized, due to its geochemical behavior and nature of its hosting rocks; its mobilization is discussed through two main topics; 1) eU/eTh ratio and 2) type and amount of mobilization.

eU/eTh ratio

The commonly recorded eU/eTh ratio for granitic rocks is about 0.33 (Clark et al., 1966; Rogers and Adams, 1969; Stuckless et al., 1977; Boyle, 1982). That ratio is considered as an important radiometric indicator to identify the fate and proximity of the U-mineralization. However, the enrichment of uranium could be indicated by increasing this ratio above 0.33

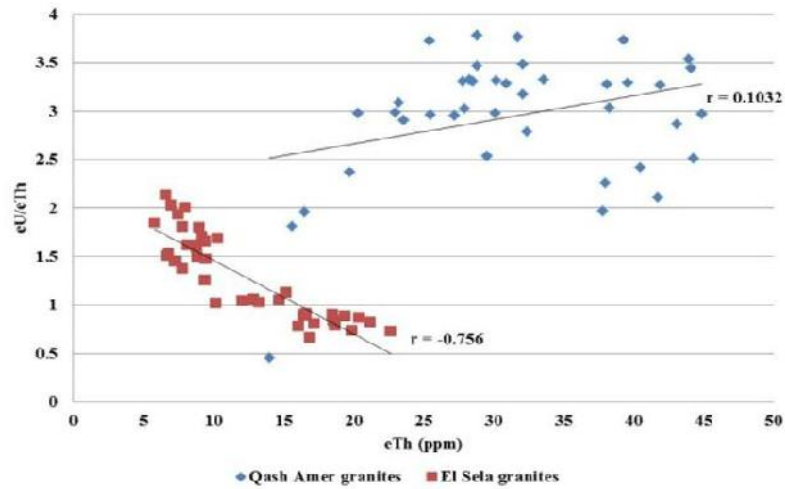


Fig. 20: eTh-(eU/eTh) binary diagrams for QA and El Sela granites

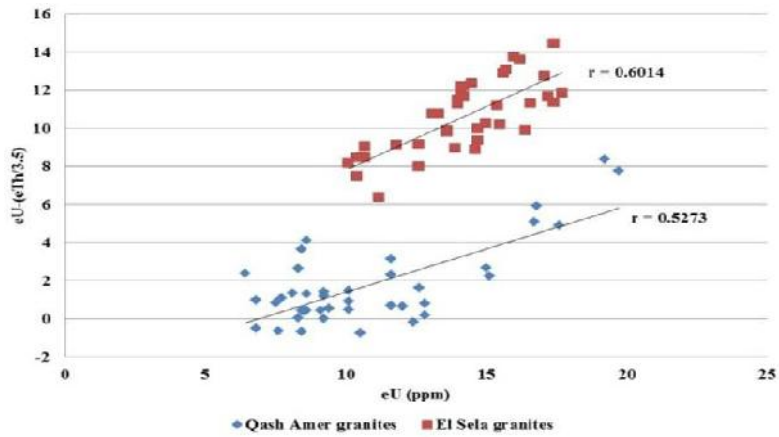


Fig. 21: eU-(eTh/3.5) binary diagrams for QA and El Sela granites

while the depleted or initially uranium poor granites could be indicated by decreasing the ratio than 0.33. The value of eU/eTh ratio in the productive uraniferous rocks is generally 1 (Darenely and Ford, 1989). The eU/eTh ratio for each rock type is quoted in Tables (1 & 2). The averages of the eU/eTh ratio are 1.29 for QA granites and 2.95 for El Sela granites, indicating uranium addition.

The radiometric studies of anomalous

samples show that their uranium contents (eU) range from 10.1 to 17.7 ppm at QA with their thorium contents (eTh) vary from 5.8 to 22.7 ppm. El Sela granites have uranium contents (eU) ranges from 6.4 to 19.7 ppm with equivalent thorium content (eTh) ranges between 14.0 and 44.9 ppm. This indicates strong post-magmatic uranium enrichment in the granitic melt. This could be supported by high concentration of uranium in accessory

Table 1: eU, eTh and K contents and their environmental parameters of Qash Amer granites

Sample No.	eU (ppm)	eTh (ppm)	K (%)	eU Bq/kg	eTh Bq/kg	K Bq/kg	Abs. Dose ^{238}U (nGy/h)	Eff. Dose (mSv)	Ra _{eq}	H _{ex}	H _{in}	I _γ
1	10.4	10.2	2.9	128.96	41.208	907.7	122.32	0.15	257.65	0.7	1.04	1.88
2	11.2	16.9	3.9	138.88	68.276	1220.7	156.3	0.19	330.32	0.89	1.27	2.42
3	11.8	9.4	3.4	146.32	37.976	1064.2	134.91	0.17	282.43	0.76	1.16	2.06
4	12.6	16.1	3.6	156.24	65.044	1126.8	158.46	0.19	335.84	0.91	1.33	2.44
5	12.6	12.1	2.8	156.24	48.884	876.4	138.25	0.17	293.49	0.79	1.22	2.11
6	13.1	8.1	3.9	162.44	32.724	1220.7	145.72	0.18	303.09	0.82	1.26	2.22
7	13.3	8.9	2	164.92	35.956	626	124.01	0.15	264.44	0.71	1.16	1.88
8	13.6	12.9	3.8	168.64	52.116	1189.4	158.99	0.19	334.58	0.9	1.36	2.44
9	13.6	13.3	3.4	168.64	53.732	1064.2	154.74	0.19	327.26	0.88	1.34	2.37
10	13.9	17.2	4	172.36	69.488	1252	173.81	0.21	367.94	0.99	1.46	2.68
11	14	9.5	3.6	173.6	38.38	1126.8	150.37	0.18	315.11	0.85	1.32	2.29
12	14	8.8	1.5	173.6	35.552	469.5	121.25	0.15	260.5	0.7	1.17	1.83
13	14.1	7.8	1.7	174.84	31.512	532.1	122	0.15	260.79	0.7	1.18	1.84
14	14.1	6.6	1.6	174.84	26.664	500.8	117.76	0.14	251.45	0.68	1.15	1.77
15	14.2	7	3.9	176.08	28.28	1220.7	149.33	0.18	310.38	0.84	1.31	2.27
16	14.2	8.8	1.4	176.08	35.552	438.2	121.1	0.15	260.58	0.7	1.18	1.82
17	14.5	7.5	1.6	179.8	30.3	500.8	122.25	0.15	261.61	0.71	1.19	1.84
18	14.6	19.9	5.1	181.04	80.396	1596.3	198.77	0.24	418.68	1.13	1.62	3.08
19	14.7	18.7	4.9	182.28	75.548	1533.7	193.8	0.24	408.18	1.1	1.6	2.99
20	14.7	16.5	4.4	182.28	66.66	1377.2	181.91	0.22	383.45	1.04	1.53	2.8
21	15	16.6	2.7	186	67.064	845.1	161.68	0.2	346.81	0.94	1.44	2.47
22	15.4	14.7	3.9	190.96	59.388	1220.7	175	0.21	369.7	1	1.52	2.68
23	15.5	18.6	5.1	192.2	75.144	1596.3	200.75	0.25	422.34	1.14	1.66	3.1
24	15.7	9.2	5	194.68	37.168	1565	177.65	0.22	368.16	1	1.52	2.71
25	15.6	9.4	1.7	193.44	37.976	532.1	134.5	0.16	288.62	0.78	1.3	2.02
26	16	8	5	198.4	32.32	1565	176.44	0.22	364.96	0.99	1.52	2.69

Table 1 Cont.

Sample No.	eU	eTh	K	eU	eTh	K	Abs. Dose ²³⁸ U(nGy/h)	Eff. Dose (mSv)	Ra _{eq}	H _{ex}	H _{in}	I _γ
27	16.2	9	5.7	200.88	36.36	1784.1	189.16	0.23	390.06	1.05	1.6	2.89
28	16.4	22.7	5.6	203.36	91.708	1752.8	222.44	0.27	469.2	1.27	1.82	3.44
29	16.6	18.5	6.4	205.84	74.74	2003.2	223.77	0.27	466.7	1.26	1.82	3.46
30	10.7	5.8	3.7	132.68	23.432	1158.1	123.74	0.15	255.24	0.69	1.05	1.89
31	10.7	7.8	1.5	132.68	31.512	469.5	99.91	0.12	213.81	0.58	0.94	1.51
32	10.6	7.3	3.7	131.44	29.492	1158.1	126.83	0.16	262.66	0.71	1.07	1.94
33	10.4	6.8	3.3	128.96	27.472	1032.9	119.24	0.15	247.66	0.67	1.02	1.82
34	10.4	10.2	2.9	128.96	41.208	907.7	122.32	0.15	257.65	0.7	1.04	1.88
35	10.1	6.7	2.3	125.24	27.068	719.9	104.23	0.13	219.29	0.59	0.93	1.59
36	17.1	15.2	3.6	212.04	61.408	1126.8	182.04	0.22	386.44	1.04	1.62	2.78
37	17.2	19.4	4.4	213.28	78.376	1377.2	203.3	0.25	431.18	1.17	1.74	3.12
38	17.4	10.3	3	215.76	41.612	939	163.97	0.2	347.44	0.94	1.52	2.48
39	17.4	21.2	48	215.76	85.648	15024	777.91	0.95	1493.81	4.04	4.62	12.31
40	17.7	20.4	5.2	219.48	82.416	1627.6	219.05	0.27	462.42	1.25	1.84	3.37
Min.	10.1	5.8	1.4	125.24	23.43	438.2	99.91	0.12	213.81	0.58	0.93	1.51
Max.	17.7	22.7	48	219.48	91.71	15024	777.91	0.95	1493.81	4.04	4.62	12.31
Av.	14.03	12.44	5.61	173.92	50.26	1755.04	184	0.23	380.94	1.03	1.5	2.83
International average				35	30	400	57	0.48	370	1	1	0.5

Table 2 : eU, eTh and K contents and their environmental parameters of El Sela granites

Sample No.	eU (ppm)	eTh (ppm)	K (%)	eU (Bq/kg)	eTh (Bq/kg)	K (Bq/kg)	Abs. Dose ^{238}U (nGy/h)	Eff. Dose (mSv)	Ra _{eq}	H _{ex}	H _{in}	I _γ
1	6.4	14	2.3	79.36	56.56	719.9	100.85	0.12	215.54	0.58	0.8	1.57
2	6.8	20.3	3.2	84.32	82.012	1001.6	130.26	0.16	278.53	0.75	0.98	2.05
3	6.8	25.4	3	84.32	102.616	939	140.09	0.17	303.15	0.82	1.05	2.21
4	7.5	23.2	3.4	93	93.728	1064.2	143.95	0.18	308.76	0.83	1.09	2.27
5	7.6	28.8	4.2	94.24	116.352	1314.6	168.63	0.21	361.58	0.98	1.23	2.67
6	7.7	23	4.2	95.48	92.92	1314.6	155.05	0.19	329.35	0.89	1.15	2.44
7	8.1	23.6	3.3	100.44	95.344	1032.9	147.06	0.18	316.1	0.85	1.13	2.31
8	8.4	31.7	4.4	104.16	128.068	1377.2	182.9	0.22	393.05	1.06	1.34	2.89
9	8.4	27.8	3.5	104.16	112.312	1095.5	161.64	0.2	348.87	0.94	1.22	2.55
10	8.4	16.5	2	104.16	66.66	626	114.49	0.14	247.54	0.67	0.95	1.78
11	8.3	28.8	4.1	102.92	116.352	1283.3	171.34	0.21	367.85	0.99	1.27	2.71
12	8.3	19.7	2.7	102.92	79.588	845.1	130.86	0.16	281.62	0.76	1.04	2.05
13	8.6	15.6	3.1	106.64	63.024	970.3	127.8	0.16	271.31	0.73	1.02	1.99
14	8.6	25.5	2.8	106.64	103.02	876.4	148.04	0.18	321.23	0.87	1.16	2.33
15	8.6	28.5	4.5	106.64	115.14	1408.5	177.55	0.22	379.47	1.03	1.31	2.8
16	8.5	28.3	4.2	105.4	114.332	1314.6	172.57	0.21	369.85	1	1.28	2.72
17	9.4	30.9	4.3	116.56	124.836	1345.9	185.38	0.23	398.43	1.08	1.39	2.92
18	9.2	27.9	3.4	114.08	112.716	1064.2	165.16	0.2	356.96	0.96	1.27	2.6
19	9.2	32.1	4.4	114.08	129.684	1377.2	188.46	0.23	405.28	1.1	1.4	2.98
20	9.2	27.2	3.7	114.08	109.888	1158.1	167.37	0.21	360.15	0.97	1.28	2.63
21	9.1	30.2	4.3	112.84	122.008	1345.9	181.95	0.22	390.67	1.06	1.36	2.87
22	10.1	30.1	3.6	125.24	121.604	1126.8	178.3	0.22	385.64	1.04	1.38	2.8
23	10.1	32.1	4.2	125.24	129.684	1314.6	191.01	0.23	411.63	1.11	1.45	3.01
24	10.1	33.6	4.9	125.24	135.744	1533.7	203.81	0.25	437.14	1.18	1.52	3.21
25	10.5	39.3	4.2	130.2	158.772	1314.6	210.87	0.26	458.14	1.24	1.59	3.33
26	11.6	29.5	4.4	143.84	119.18	1377.2	195.87	0.24	420.04	1.14	1.52	3.07

Table 2: Cont.

Sample No.	eU	eTh	K	eU	eTh	K	Abs. Dose ^{238}U (nGy/h)	Eff. Dose (mSv)	Ra _{eq}	H _{ex}	H _{in}	I _γ
27	11.6	32.4	3.8	143.84	130.896	1189.4	195.11	0.24	422.33	1.14	1.53	3.06
28	11.6	38.1	5.5	143.84	153.924	1721.5	231.21	0.28	496.15	1.34	1.73	3.65
29	12	39.6	5.1	148.8	159.984	1596.3	231.94	0.28	500.14	1.35	1.75	3.66
30	12.4	43.9	5.2	153.76	177.356	1627.6	246.03	0.3	532.33	1.44	1.85	3.88
31	12.6	38.3	4.3	156.24	154.732	1345.9	221.77	0.27	480.82	1.3	1.72	3.49
32	12.8	41.9	5.2	158.72	169.276	1627.6	243.44	0.3	525.74	1.42	1.85	3.84
33	12.8	44.1	5.1	158.72	178.164	1596.3	247.51	0.3	536.03	1.45	1.88	3.9
34	15	43.1	5.9	186	174.124	1846.7	268.11	0.33	576.8	1.56	2.06	4.21
35	15.1	44.9	5.4	187.24	181.396	1690.2	266.55	0.33	576.39	1.56	2.06	4.19
36	19.2	37.8	4.5	238.08	152.712	1408.5	260.97	0.32	564.59	1.53	2.17	4.05
37	19.7	41.7	5.3	244.28	168.468	1658.9	283.79	0.35	612.56	1.66	2.32	4.42
38	34.4	24.6	4.8	426.56	99.384	1502.4	319.75	0.39	684.11	1.85	3	4.84
39	16.7	40.5	6	207.08	163.62	1878	272.81	0.33	585.28	1.58	2.14	4.27
40	16.8	38	5.2	208.32	153.52	1627.6	256.84	0.31	552.83	1.49	2.06	4.01
Min.	6.4	14	2	79.36	56.56	626	100.85	0.12	215.54	0.58	0.8	1.57
Max.	34.4	44.9	6	426.56	181.4	1878	319.75	0.39	684.11	1.85	3	4.84
Av.	11.64	30.99	4.18	144.37	125.18	1308.64	195.42	0.24	420.56	1.14	1.53	3.06
International average				35	30	400	57	0.48	370	1	1	0.5

minerals (e.g., zircon, fluorite and radioactive minerals (e.g., uranophane, autonite and meta-autonite) and adsorbed mostly by iron oxides (Ali et al., 2008).

Type and Amount of Uranium Mobilization

The uranium mobilization rate (P) is calculated by $P = U_m/U_p \times 100\%$. The obtained results of U_o , U_m and P for representative samples of the studied rocks are listed in Table 3. Dynamics of uranium-rich fluids and amount of mobilized uranium as well as uranium mobilization rate in the studied rocks are calculated through several steps using equations of Benzing Uranium Institute of

China and CNNC (1993). The paleo-uranium background (the original uranium content) is calculated by $U_o = eTh \times eU/eTh$ (17.96 for QA and 31.28 for El Sela granites), where: U_o is the original uranium content, eTh is the average of thorium content in certain geologic unit and eU/eTh is the average of the regional eU/eTh ratio in different geologic units.

The amount of the mobilized (migrated) uranium (U_m) is calculated by $U_m = U_p - U_o$, where, U_m is the amount of the mobilized uranium and U_p is the average of the present uranium content in certain geologic unit. If $U_m > 0$: this means that U was gained or mobilized into the geologic body during late evolution (migration in or enriched). If $U_m < 0$: this means that U had been lost from the

Table 3 : The Benzing parameters for Qash Amer and El Sela granites

Parameter	Uo	Up	Um	P
Qash Amer granites	17.97	14.03	-3.93	-28.01
El Sela granites	31.28	10.79	-20.49	-189.9

geologic body during late evolution (migration out or depletion). The data reveals that the Um values are <0 in QA granites (-3.93) with migration rate (P) -28.01 and El Sela granites (-20.49) with migration rate -189.9 indicating that U was mobilized out from them (migration out), mostly to the shear zone cutting through the area.

ENVIRONMENTAL IMPACTS

Granitic rock samples are used in some industrial applications such as utilization of these rocks as an ornamental stones and in building materials. Physiomechanical characterization detected to determine their suitability for uses as an ornamental stones. All rocks passes the tests and suitable as ornamental stones (Lasheen, 2019).

Absorbed Dose Rate in Air (D)

The absorbed gamma dose rates in air at 1m above the ground surface for the uniform distribution of radionuclides (²³⁸U, ²³²Th and ⁴⁰K) were calculated by using Equation 1 on the basis of guide lines provided by UNSCEAR (2000) and rgiin et al., (2007).

$$D \text{ (nGy/h)} = 0.462A_U + 0.604A_{Th} + 0.0417A_K \quad (1)$$

where A_U, A_{Th} and A_K are the average specific activities of ²²⁶Ra, ²³²Th and ⁴⁰K in Bq/kg, respectively.

Annual Effective Dose Equivalent (AEDE)

The annual effective dose equivalent (AEDE) was calculated from the absorbed dose by applying the dose conversion factor of 0.7 Sv/Gy and the outdoor occupancy factor of 0.2 (UNSCEAR, 2000; rgiin et al. 2007).

Radium Equivalent Activity (Raeq)

The radium equivalent activity for the samples was calculated. The exposure to radiation (Tufail et al., 1992) can be defined in terms of the radium equivalent activity (Ra_{eq}), which can be expressed by the following equation:

$$Ra_{eq} = A_{Ra} + 10/7A_{Th} + 10/130A_K \quad (2)$$

where A_{Ra}, A_{Th} and A_K are the specific activities of Ra, Th and K, respectively, in Bq kg⁻¹.

External and Internal Hazard Index (H_{ex} and H_{in})

To limit the annual external gamma-ray dose (Saito and Jacob, 1995 and UNSCEAR, 2000) to 1.5 Gy for the samples under investigation, the external hazard index (H_{ex}) is given by the following equation:

$$H_{ex} = A_U/370 + A_{Th}/259 + A_K/4810 \quad (3)$$

The internal exposure to ²²²Rn and its radioactive progeny is controlled by the internal hazard index (H_{in}), which is given by Nada (2003).

$$H_{in} = A_U/185 + A_{Th}/259 + A_K/4810 \quad (4)$$

These indices must be less than unity in order to keep the radiation hazard insignificant (Lakehal et al., 2010; Baykara et al., 2010).

Activity Concentration Index (I)

Another radiation hazard index called the representative level index, **I** , is defined as follows (NEA-OECD, 1979):

$$I_\gamma = A_U/150 + A_{Th}/100 + A_K/1500 \quad (5)$$

where A_U , A_{Th} and A_K are the activity concentrations of ^{226}Ra , ^{232}Th and ^{40}K , respectively in Bq kg^{-1} (Abbady et. al., 2005). The safety value for this index is 1 (El Galy et al., 2008; El Aassy et al., 2012; Harpy et al. 2019b; Taha et al., 2020).

The average absorbed dose rate (D) values for the studied granitic rocks of QA and El Sela are shown in Tables 2 and 3. The calculated values of the studied samples vary between 99.91 and 777.91 nGyh^{-1} with an average 184.00, 100.85 and 319.75 with an average 195.42 nGyh^{-1} in QA and El Sela, respectively. These estimated values of absorbed dose rate in the studied samples are comparably higher than the world average value 57 nGyh^{-1} (Harpy et al., 2019b; Taha et al., 2020).

On the other hand, the average values of annual effective dose for the studied samples were also listed. The values obtained varied between 0.12 and 0.95, 0.12 and 0.39 mSv^{-1} for QA and El Sela granitic samples, respectively. The mean value 0.23 and 0.24 for the two localities, respectively which found to be less than 0.48 mSv^{-1} recommended by UNSCEAR (2000) as the worldwide average of the annual effective dose.

The radium equivalent activity R_{eq} for QA and El Sela samples ranged between 213.81 and 1493.81 Bq Kg^{-1} with 380.94, Bq Kg^{-1} , 215.54 and 6.84.11 Bq Kg^{-1} with 420.56, Bq Kg^{-1} as a mean value, respectively which was to some extent higher than the maximum permitted value (370 Bq Kg^{-1}).

The values of internal hazard indices (H_{in}) for the studied QA and El Sela samples ranged between 0.58 and 4.04, 0.58 to 1.85, respectively, while the external hazard index varies between 0.93 and 4.62, 0.80 and 3.00, respectively. External and internal hazard indices were significantly higher than unity for most of the studied samples suggesting that these granitic rocks couldn't be used as building and interior decorative material of dwelling.

The gamma activity index (I) used to assess safety requirement for the studied rocks

were evaluated and presented in Tables 2&3. The obtained values for both localities ranged between 1.51 and 12.31 with average 2.83, 1.57 and 4.84 with average 3.06, respectively. The obtained values of gamma activity indices in all granitic rock samples were higher dose criterion (0.3 mSv/y) and/or some samples are higher than an activity concentration index of 2 I 6 for materials used in bulk construction.

CONCLUSIONS

El Sela area is mainly covered by ophiolitic mélange (Sul Hamed), biotite granites, two-mica granite (El Sela) muscovite granites (Qash Amer), and different types of acidic and basic dikes as well as quartz and jasper veins. The field studies indicated that the granitic rocks are suffered from hydrothermal alterations, especially around ENE-WSW and NNW-SSE El Sela shear zones, that affected by hydrothermal alterations in post-granitic dikes as well as quartz and jasper veins accompanied by radioactive mineralization. Microscopically, granites are composed essentially of alkali feldspar, quartz, muscovite and biotite. Accessories are represented mainly by zircon, monazite, apatite, fluorite and iron oxides. Secondary uranium minerals are represented by uranophane, autunite, meta-autunite and phurcalite. The radiometric studies of the samples show that their uranium contents (eU) range from 10.1 to 17.7 ppm at Qash Amer with their thorium contents (eTh) vary from 5.8 to 22.7 ppm. El Sela granites have uranium contents (eU) ranges from 6.4 to 19.7 ppm with equivalent thorium content (eTh) ranges between 14.0 and 44.9 ppm. This indicates strong post-magmatic uranium enrichment in the granitic melt. Recent studies clarify that the chemically determined uranium is to a great extent higher than the radiometrically obtained results suggesting El Sela uranium could be considered as recent uranium deposits and this confirm their hazard. Mobilization studies of uranium indicate that its mobilization out (migration out), mostly to the shear zone cutting through

the area. Though the suitability of these rocks for using as ornamental stones, most samples have radiological parameters values higher than the international standards suggesting that G. El Sela granitic rocks are hazard for use as ornamental stones.

RECOMMENDATIONS

It obvious that from the present work, the authors recommend that the inhabitants at El Sela and Qash Amer granites could be spread horizontally through out these granites, because they were not considered as safety environments and not recommended to be used in building materials as an ornamental stones. They have radiological parameters values higher than the international recommended values that exceed the world permissible value.

REFERENCES

- Abbadly, A. G.; Uosif, M. A., and El-Taher, A., 2005. Natural radioactivity and dose assessment for phosphate rocks from Wadi El-Mashash and El-Mahamid Mines, Egypt. *J. Envir. Radio.*, 84 (1), 65–78.
- Abdalla, H. M.; Matsueda, H.; Ishihara, S., and Miura, H., 1994. Mineral chemistry of albite-enriched granitoids at Um Ara, Southeastern Desert, Egypt. *Int. Geol. Rev.*, 36, 1067–1077.
- Abdel Gawad, A.E., 2018. Geochemical behaviour of trace and rare earth elements during hydrothermal alteration at El Sela shear zone, Egypt. VIII young geoscientists school, New knowledge about ore-forming processes , IGEM RAS. Moscow, 439–442.
- Abdel Gawad, A.E., and Ibrahim E.M., 2016. Activity ratios as a technique for studying uranium mobility at El Sela shear zone, southeastern Desert, Egypt. *Radioanalytical Nuc. Chem.*, DOI 10.1007/s10967-015-4374-0, 129–142.
- Abdel Gawad, A.E.; Orabi, A.H., and Bayoumi M.B., 2015. Uranium evaluation and its recovery from microgranite dike at G. El Sela area, south Eastern Desert, Egypt. *Arab. J. Geosci.*, DOI 10.1007/s12517-014-1499-3, 4565–4580.
- Abdel Meguid A. A.; Ammar, S. E.; Ibrahim, T. M. M.; Ali K. G.; Shahin, H. A.; Omer S. A.; Gaafar I. M. E.; Masoud S. M.; Khamis, A. A.; Haridy, M. H.; Kamel, A. I.; Mostafa, B. M.; Abo Donia A.; Abdel Gawad, A. E., and Aly E. M., 2003. Uranium Potential of Eastern Desert Granites, Egypt. NMA report for Model project EGY/03/014 sponsored by IAEA 270 p.
- Abdel Naby, H.; Frisch, W., and Siebel, W., 2008. Tectono-metamorphic evolution of the Wadi Hafafit Culmination (central Eastern Desert, Egypt). Implication for Neoproterozoic core complex exhumation in NE Africa. *Geologica Acta*, 6, N° 4, 293-312
- Abu Dief, A., 1985. Geology of uranium mineralization in El-Missikat area, Eastern Desert, Egypt. M.Sc. Thesis, Fac. Sci., Al-Azhar Univ., 103 p.
- Abu-Deif, A., 1992. The relation between the uranium mineralization and tectonics in some Pan-African granites, west of Safaga, Eastern Desert, Egypt. Ph.D. Thesis, Assiut Univ., Egypt, 218 p.
- Abu Zeid, E.A., 2020. Autunite-group minerals and their paragenesis from the sheared granite of Gabal El Sela, south Eastern Desert, Egypt. *Open J. Geol.*, 10, 703–725.
- Abu El Laban, S. A. 2002. Some geological and geochemical studies in Abu Ramad area, South Eastern Desert, Egypt. Ph.D. Theses, Fac. Sci. Ain Shams Univ. Egypt.
- Ali, K. G., 2013. Structural control of El Sela granites and associated uranium deposits, south Eastern Desert, Egypt. *Arab J Geosci*, 6(6), 1753–1767.
- Assaf, H. S.; Mahdy, M. A., and El-Afandy, A. H., 1997. Egyptian Younger Granites; an approach to define parameters favoring formation of uranium deposits. 3rd Int. Conf. Geochem.,

- Alex. Univ. Egypt, 409–420.
- Baykara, O.; Karatepe, S., and Do ru, M., 2010. Assessments of natural radioactivity and radiological hazards in construction materials used in Elazig, Turkey. Technical Report. Radiat. Meas. doi: 10.1016 / J. Radmeas. 2010.08.010.
- Bentor, Y. K., 1985. The crustal evolution of the Arabo-Nubian massif with special reference to the Sinai Peninsula. *Precambrian Res.* 28, 1–74.
- Benzing Uranium Institute, 1977. Field Gamma-Ray Spectrometric Survey No. 3, 1:292, China.
- Beyth, M.; Stern, R. J.; Altherr, R., and Kro ner, A., 1994. The late Precambrian Timna igneous complex, Southern Palestine: Evidence of comagmatic-type sanukitoid monzodiorite and alkali granite magma. *Lithos*, 31, 103–124.
- Boyle, R. W., 1982. Geochemical prospecting for thorium and uranium deposits, *Develop. Econ. Geol.*, 16, Elsevier, Amsterdam. 508p.
- China National Nuclear Corporation (CNNC), 1993. Research achievement from Bureau of Geology. Internal report, China.
- Clark, S. P. Jr.; Peterman, Z. E., and Heier, K. S., 1966. Abundances in uranium, thorium and potassium. In: *Handbook of Physical Constants*, Geol. Soc. Amer., Memoir No. 97, 521–541.
- Cuney, M.; Leroy, J., and Molina, P., 1989. Metallogenesis in the French part of the Variscan orogen. Part 1. U-preconcentrations in the pre-Variscan and Variscan formations-A comparison with Sn, W and Au. *Tectonophysics*, 177, 39–57.
- Darenely, A. G., and Ford, K. I., 1989. Regional airborne gamma-ray survey; a review. In: *Proceedings of 3rd Inter. Conf. Geoph. and Geoch. Exploration for Minerals and Ground Water. I.3.*, Geol. Sur., Ontario, 229–240.
- El Aassy, I. E.; Nada, A. A.; El-Galy, M. M., and El-Feky, M. G., 2012. Behavior and environmental impacts of radionuclides during the hydrometallurgy of calcareous and argillaceous rocks, southwestern Sinai, Egypt. *Applied radiation and isotopes*, 70(6):1024–1033.
- El Galy, M. M.; El Mezayn, A. M.; Said, A. F., and El Mowafy, A. A., 2008. Distribution and environmental impacts of some radionuclides in sedimentary rocks at Wadi Naseib area, southwest Sinai, Egypt. *J. Env. Radio.*, 99(7), 1075–82.
- El Mezayen, A. M.; Heikal, M. A.; Abu Zeid I. K.; Omar, S. A.; El-Feky, M. G., and Lasheen, S. R., 2017. Petrography, geochemistry and radioactivity of El-Gidami granitic Rocks, Central Eastern Desert, Egypt. *Al Azhar Bull. Sci.*, 9th, Conf., 25–40.
- El-Nisr S. A.; El-Sayed M. M., and Saleh, G. M., 2002. Geochemistry and petrogenesis of Pan-African late- to post-orogenic younger granitoids at Shalatine-Halaib, South Eastern Desert, Egypt. *J. Afr. Earth Sci.*, 33, No.2, 261–282.
- Gaafar, I. M., 2005. Applications of Geological and Geophysical Survey for Defining the Uranium Potentiality of Some Younger Granites in the Eastern Desert of Egypt. Ph. D. Thesis, Fac. Sci., Mansoura Univ., Egypt, 180p.
- Gaafar, I. M.; Hosni H.; Ghazala, H. H.; Ibrahim T. M., and Ammar, S. E., 2006. Gamma-Ray spectrometry studies for A Promising Vein Type Uranium Mineralization, South Eastern Desert, Egypt. *Proc. 4th Inter. Symposium on Geoph.*, Tanta, 2006, 445–456.
- Greiling, R. O.; Abdeen, M.; Dardir, A.; El Akhal, H.; El Ramly, M. F.; Kamal El Din, G. M.; Osman, A. F.; Rashwan, A. A.; Rice, A. H., and Sadek. M. F., 1993. A structural synthesis of the Proterozoic Arabian-Nubian Shield in Egypt. *Geologische Rundschau*, 83(3), 484–501.
- Harpy, N. M.; El Dabour, S. E.; Sallam, A. M.; Nada, A. A.; El Aassy, A. E., and El-Feky, M. G. 2019. Environmental forensics, doi:10.1080/15275922,1695020.
- Hassan, M. A., and Hashad, A. H. 1990. Precambrian of Egypt. *The Geology of Egypt*,

- Rotterdam/Brookfield: A. A. Balkema, 201-245.
- Hussein, H. A.; Hassan, M. A.; El Tahir, M. A., and Abu-Deif, A., 1986. Uranium bearing siliceous veins in younger granites, Eastern Desert, Egypt. Report of the Working Group on Uranium Geology, IAEA, Vienna, TECDOC. 361, 143–157.
- Ibrahim, M. E., 1986. Geologic and Radiometric Studies on Um Ara Granite Pluton, South East Aswan, Egypt. M.Sc. Thesis, Mansoura Univ., Egypt.
- Ibrahim, T. M., 2002. Geologic and Radioactive Studies of the Basement-Sediment contact in the Area West Gabal El Missikat- Eastern Desert, Egypt. Ph. D. Thesis, Fac. Sci., Mansoura Univ., Mansoura, Egypt.
- Ibrahim, T. M. M.; Cuney, M.; Ali, K. G.; Abdel Meguid, A. A.; Gaffar, I. M.; Shahin H.; Omar, S. A.; Masoud, S. M., and Haridy, H. M. M., 2005. The U-fertility Criteria Applied to El Sela Granite, South Eastern Desert, Egypt. Inter. Symp. Uranium Prod. and Raw Materials for the Nuclear Fuel Cycle, IAEA, Vienna, Austria, 100–103.
- Jiashu, R., and Zehong, H., 1982. Forms of Uranium occurrence and its distribution in uraniferous granites. In: *Geology of Granites and their Metallogenetic Relations*, Sciences Press, Beijing, 621–635.
- Khalaf, I. M., 2005. Geology of the area around G. Qash Amer with special emphases on the granitic rocks, south Eastern Desert, Egypt. *Egyptian J. Geol.*, 49, 49-64.
- Killeen, P. G., and Cameron, G. W., 1977. Computation of in situ potassium, uranium and thorium concentrations from portable gamma-ray spectrometer data. In: *Report of Activities*, part A. *Geol. Surv. Can.*, Paper 77-1A, 91–92.
- Lasheen, E.R., 2019. Petrology, Geochemistry of the Pan-African rocks at Soul Hamed area, South Eastern desert, Egypt and their suitability for some industrial applications, PhD Thesis, AL-Azhar Univ., 329P.
- Lakehal, C. H.; Ramdhan, M., and Boucenna, A., 2010. Natural radionuclide concentrations in two phosphate ores of east Algeria. *J. Envir. Radioactivity*, 101(5),377-9.
- Mira, H. I., and Ibrahim, T. M., 2009. Mineralogical and geochemical evidence for tetravalent uranium mineralization within El Sela weathered granite, South Eastern Desert, Egypt. *Annals Geol. Surv. Egypt*. XXXI.
- Nada, A., 2003. Evaluation of natural radionuclides at Um-Greifat area, Eastern Desert of Egypt. *Appl. Radiat. Isot.*, 58, 275–280.
- NEA-OECD, 1979. Exposure to Radiation from Natural Radioactivity in Building Materials. Report by NEA Group of Experts of the Nuclear Energy Agency, OECD, Paris, France.
- rgün Y.; Altunsoy N.; Ahin S. Y.; Güngör Y.; Gültekin A. H.; Karahan G., and Karacık Z., 2007. Natural and anthropogenic radionuclides in rocks and beach sands from Ezine region (Canakkale), Western Anatolia, Turkey. *App. L Radiat. Isot* 65,739–747.
- Rashed, M. A., 2001. Geology, petrology and uranium potential of G. Qash Amer–G. El Sela granitic mass, South Eastern Desert, Egypt. M.Sc. Thesis, Mansoura Univ., 120 p.
- Rogers, J. J. W., and Adams, J. A. S., 1969. Uranium and Thorium, In: Wedepohl, K.H., Ed., *Handbook of Geochemistry*, 113, Springer, Berlin, 92-B-1 to 92-0-8 and 90-Bb-1 to 90-00-5.
- Roz, M. E., 1994. Geology and Uranium Mineralization of Gabal Gattar Area, North Eastern Desert, Egypt. M.Sc. Thesis, Al Azhar Univ., Egypt, 175 p.
- Saito, K., and Jacob, P., 1995. Gamma Ray fields in the air due to sources in the ground. *Radiation Protection Dosimetry*, 58 (1),29–45.
- Saleh, G. M.; Afify, A. M.; Emad, B. M.; Dawoud, M. I.; Shahin, H. A., and Khaleal, F. M., 2019. Mineralogical and geochemical characterization

- of radioactive minerals and rare earth elements in granitic pegmatites at G. El Fereyid, South Eastern Desert, Egypt. *J. Afri. Earth Sci.*, 160, 103651.
- Shahin, A. A., 2014. Zr-Y-Nb-REE mineralization associated with microgranite and basic dykes at El Sela shear zone, South Eastern Desert, Egypt. *Springer plus*, 3,573.
- Shahin, A. H., 2011. Occurrence of uraniferous iron and manganese oxides in biotite granite North East Gabal El Sela area, South Eastern Desert, Egypt, *Arabian J. Geosciences*.
- Stern, R. J., 1994. Arc Assembly and Continental Collision in the Neoproterozoic East African Orogen: Implications for the consolidation of Gondwanaland. *Annual Reviews Earth Planetary Sciences*, 22, 319–351.
- Stern, R. J., and Hedge, C. E., 1985. Geochronologic and isotopic constraints on late Precambrian crustal in the Eastern Desert of Egypt. *Am. J. Sci.*, 285, 97–127.
- Stern, R. J., and Gottfried, D., 1986. Petrogenesis of a Late Precambrian (575–600 Ma) bimodal suite in Northeast Africa. *Contrib Mineral Petrol*, 92, 492–501.
- Stuckless, H. S.; Bunker, C. M.; Bush, C. A.; Doering, W. P., and Scott, J., 1977. Geochemical and petrologic studies of a uraniferous granites of the Granite Mountains, Wyoming, US. *Geol Surv J. Res*, 5,61–81.
- Taha, S. H.; Sallam, O. R.; Abbas, A. A., and Abed, N. S., 2020. Radioactivity and environmental impacts of ferruginous sandstone and its associating soil. *Inter. J. Envir. Analytical Chem.*, 1–10.
- Tufail, M.; Siddiqui, M. S.; Ali, S., and Mirza, N. M., 1992. Investigation of gamma-ray activity and radiological hazards of the bricks fabricated around Lahore (Pakistan). *Pakistan J. Sci. Indus.Res.*, 34(6),216–220.
- UNSCEAR, 2000. Sources and effects of ionizing radiation. Report to the General Assembly of the United Nations with Scientific Annexes, United Nations

التأثيرات الإشعاعية والبيئية لجرانيتات سيلا - قش عامر، جنوب الصحراء الشرقية، مصر

سامح زكريا توفيق، محمد أحمد شاهين و مصطفى سعد السطوحي

منطقة سيلا مغطاة بصورة رئيسية بمزيج صول حامد الأوفيليتي، جرانيت بيوتيتي، جرانيت سيلا ثنائي البيوتيت، جرانيت قش عامر المسكوفيتي بالإضافة الى تقاطعات من الجرانيت الدوليريتي الدقيق وجدد البوستونايت مع عروق الكوارتز والعقيق. صخور الجرانيت هذه متحولة بالمحاليل الحارة المصاحبة للتمعدنات المشعة خاصة حول نطاق التهشم بجبل سيلا باتجاه شرق شمال شرق- غرب جنوب غرب. تتكون هذه الصخور بشكل رئيسي من الفلسبار القلوي، الكوارتز، المسكوفيت والبيوتيت بالإضافة للزركون والفلورايت والأباتيت وأكاسيد الحديد كمعادن ثانوية. المعادن المشعة تتمثل في اليورانوفين، الأوتونايت، والأوتونايت المتحول والفيوركالسيت والتي تتواجد بصورة حصرية بالجرانيتات الدقيقة شديدة التهشم وجدد الدوليريت وعروق العقيق. تتراوح محتويات اليورانوم بقش عامر بين جزء بالمليون بينما محتوى الثوريوم يتراوح بين جزء بالمليون بينما محتوى اليورانوم بجرانيتات سيلا يتراوح بين جزء بالمليون بينما محتوى الثوريوم يتراوح بين

بالمليون. تظهر العلاقات الثنائية المختلفة للعناصر المشعة وجود اضمحلال في اليورانيوم بكلا منطقتي الدراسة (سيلا وقش عامر) مفترضة حدوث انتزاع لليورانيوم من الصخور الأصلية الحاوية له نحو نطاق التهشم المتجه شرق شمال شرق-غرب جنوب غرب وشمال شمال غرب-جنوب جنوب شرق. تم حساب كمية اليورانيوم المهاجر واتجاهه سواء لداخل مناطق الدراسة أو لخارجها وتبين انها باتجاه نطاق التهشم المار بالمنطقتين. تم كذلك حساب جرعات التعرض الاشعاعي وجرعة التعرض بالعام ونشاط الراديوم ومعامل الخطورة ومعامل نشاط أشعة جاما والتي دلت على أن كلا من منطقة سيلا وقش عامر يعطيان قراءات أعلى من معدلات الأمان العالمية مما يعتبرهما منطقتين غير مناسبتين للاقامة أو لاستخدام الصخور الجرانيت بهما في البناء أو الزينة.